Visual Object Tracking for the Extraction of Multiple Interacting Plant Root Systems

Stefan Mairhofer[1,3(✉)], Craig J. Sturrock[1,2], Malcolm J. Bennett[1,2], Sacha J. Mooney[1,2], and Tony P. Pridmore[1,3]

[1] Centre for Plant Integrative Biology, University of Nottingham, Nottingham, UK
stefan.mairhofer@nottingham.ac.uk
[2] School of Biosciences, University of Nottingham, Nottingham LE12 5RD, UK
[3] School of Computer Science, University of Nottingham, Nottingham NG8 1BB, UK

Abstract. We propose a visual object tracking framework for the extraction of multiple interacting plant root systems from three-dimensional X-ray micro computed tomography images of plants grown in soil. Our method is based on a level set framework guided by a greyscale intensity distribution model to identify object boundaries in image cross-sections. Root objects are followed through the data volume, while updating the tracker's appearance models to adapt to changing intensity values. In the presence of multiple root systems, multiple trackers can be used, but need to distinguish target objects from one another in order to correctly associate roots with their originating plants. Since root objects are expected to exhibit similar greyscale intensity distributions, shape information is used to constrain the evolving level set interfaces in order to lock trackers to their correct targets. The proposed method is tested on root systems of wheat plants grown in soil.

Keywords: Multiple object tracking · Root system recovery · Plant interaction · X-ray micro computed tomography

1 Introduction

Image analysis methods have become an inherent part of many plant biological studies, assisting researchers in extracting and processing information implicit in collected image data. The focus can vary from specific plant organs [6,22] to whole individual plants [3]. In this work we are interested in the below-ground portion of the plant, its root system. It has been shown that plants rely on their roots for water and nutrient uptake, which largely determine their performance and development [15]. We focus on the analysis of multiple interacting plants, as their root systems can facilitate either cooperative or competitive interactions. This is provided, for instance, by influencing the composition of the bacterial flora in the rhizosphere, which may positively affect the nutrient availability, or by competing for (limited) resources [26].

When roots are to be examined, they are usually either destructively removed from their environment [31] or grown in artificial media [5], which may alter their

L. Agapito et al. (Eds.): ECCV 2014 Workshops, Part IV, LNCS 8928, pp. 89–104, 2015.
DOI: 10.1007/978-3-319-16220-1_7

natural growth behaviour due to the lack of complex biological, chemical and physical properties usually found in soil [10]. An alternative solution that allows roots to be imaged in soil is given by X-ray micro computed tomography (μCT), which is becoming increasingly accessible [19]. An additional advantage to its non-disruptive characteristic [35] is the acquisition of three-dimensional volumetric image data, which allows a more accurate quantification of root system traits. Plant root systems are complex, highly branched structures, composed of many individual roots of varying size. Recovering the fine and complex structure from μCT image data presents a challenging problem in image analysis. The process is complicated by the highly heterogeneous growth environment, composed of minerals, soil particles, organic matter, water and air filled pores.

In this work we present a visual object tracking framework that allows the extraction of interacting plant root systems from their soil environment. A given data volume can be horizontally sliced into thin cross-sections to obtain a stack of images. Using a level set method guided by a greyscale intensity distribution model, it is possible to **identify the boundaries of root cross-sections** in each image. When traversing these images in sequence, root objects will appear at slightly different positions due to the root's slanted growth through the soil environment. The architectural structure of plant root systems is found by **following individual root cross-sections** through a sequence of image slices. This is achieved using an adaptive appearance model of the target and readjusting the interface of the level set function to the new location and outline of the root object. In the presence of multiple root systems, multiple trackers can be used but **root cross-sections need to be distinguished from one another** in order to allow the correct labelling of different plants. However, because all root objects are likely to have similar greyscale intensity values, their appearance models can be expected to be similar or even identical. If two or more independently tracked targets interact, their trackers can easily drift away to the object that best fits the model [12]. This can often result in an uncontrolled behaviour in which trackers switch their targets or trackers follow the same target while losing hold of others. In case of root extraction, this can lead to root cross-sections being assigned to incorrect root systems. To address the problem, a shape constraint is added to the evolving interface of the level set function during the period of target interaction.

In what follows we give a brief overview of related work on the extraction of root-structure-like networks with focus on X-ray CT (Section 2) and give a detailed description of our proposed method (Section 3). The extraction method is first applied to volume data of individual and then of multiple interacting root systems of winter wheat Cordiale (*Triticumaestivum L.*) (Section 4), followed by discussion and conclusions (Section 5).

2 Related Work

Using a high energy X-ray CT scanner, Heeraman et al. [9] endeavoured to image and quantify the root system of plants grown in sand culture. With this they were

among the first who showed that roots can be separated from non-root material on a computational basis and not just by human assumption of the presence of roots. A number of voxels were manually selected to define groups of different components (air, roots, sand). These were tested for normality and used to statistically classify the remaining voxels to one of these groups. The method does not guarantee connectivity and outlier voxels can easily be assigned to incorrect components. Seeking to advance imaging and analysis procedures, Lontoc-Roy et al. [14] presented methods and results obtained using X-ray CT for soil-root studies. Roots were segmented from the images by choosing visually a lower and upper threshold value. The resulting segmentation included primarily larger roots. In a second step, an iterative three-dimensional region growing method was used, appending voxels that are connected to the initial extraction, but which also fall within a second, wider, threshold boundary. A similar approach is reported by Perret et al. [20]. To extract the root system from the growth media, a predefined threshold boundary was applied after which a 26-neighbour connectivity constraint was imposed. While this guarantees connectivity of the root system, thresholding only gives satisfactory results if the greyscale values of different components do not overlap, in our experience this is often not the case. In the work presented by Pierret et al. [21], image slices were first segmented using a combination of thresholding and a top-hat filter [18]. By superimposing two consecutive images, extracted root cross-sections were tested for continuity while roughly defining the roots' skeleton. Since elliptical objects were prone to artefacts, they were ignored in the analysis, which had the disadvantage of missing out horizontally growing roots. The authors were aware of this limitation, but considered it a reasonable compromise, leaving the method useful for preliminary investigations. Quantification was made based on the extracted skeletons. To overcome the limitation of thresholding for overlapping greyscale intensity distributions, Kaestner et al. [11] applied a non-linear diffusion filter multiple times with different parameters to smooth out the texture of the sand matrix. As a result, the intensity distribution of root material was shifted to the tail of the sand distribution, making Rosin's unimodal thresholding algorithm applicable [24]. To remove misclassified voxels, a dilation by reconstruction operation [33] was applied to eliminate speckles while at the same time preserving thin root segments and enforcing connectivity of the root system. Filtering the data does not always result in the distribution of root material being shifted to the tail of the background distribution. The effect depends on the condition and composition of the soil matrix. Even though the methods presented by Pierret et al. [21] and Kaestner et al. [11] make use of thresholding to perform an initial crude segmentation, additional rules are applied to help decide whether an extracted object reflects the characteristics of a root segment.

Using an electron beam X-ray CT scanner, Sonka et al. [30] presented in their work a method able to identify airway trees in lungs, which, compared to plant root systems, share a similar structure. Analogous to the method presented by Lontoc-Roy et al. [14], a conservative threshold was chosen for a three-dimensional region-growing to recover the primary tree of the airway structure without the fine segments of smaller diameter. To enhance the fine details of

small airways, the image was scaled by a factor of 2 and enhanced using a top hat transform [29]. Using edge-based region-growing, the enhanced image was segmented into airways, vessels and background corresponding to dark, bright and intermediate greyscale values. A rule-based analysis using prior knowledge of the anatomical structure of airways and their relationship with pulmonary vascular trees, was used to refine the segmentation. Although prior knowledge of root system structures could be useful in their recovery, linking root segments to their environment is not straightforward. An alternative method for the extraction of airways from electron beam X-ray CT image data, was presented by Aykac et al. [1], whose method is based on mathematical morphology which was also a key component in Kaestner et al.'s presented method [11]. A greyscale morphological reconstruction was used to identify local minima in cross-sectional images, which correspond to potentially fine airway segments. The image was then thresholded using a relative value that lies between the minimum and maximum greyscale values. This process was repeated a number of times using different sized morphological structure elements. The union of all candidate regions found were used for reconstructing the airway tree. While using morphological operations can enhance fine details in the image data, it cannot completely overcome the limitations of threshold based segmentation. In addition to methods based on region growing [30] or mathematical morphology [1], solutions were proposed that use a tracing strategy [32].

This was also found to be successful in the extraction of three-dimensional and root-structure-like networks outside of X-ray CT imaging. Flasque et al. [7] for instance, used magnetic resonance angiography (MRA) for imaging cerebral blood vessels and developed a centreline tracing based method for their extraction. The centreline was traced stepwise, with successive points being estimated by searching within an orientated parallelepiped around previously identified points. Rules, like the definition of a maximum allowed curvature, were imposed for each search area. Such a rule-based concept allows the specification of a profile that is based on prior knowledge. To deal with the detection of junctions or branches, the number of entry and exit points along the surface of each parallelepiped is noted. By the definition of a continuous vessel, a parallelepiped must have exactly one entry and exit point. If more than one exit point is detected, then the presence of a junction is assumed, for which a new starting point is created. In a final step, all traced centreline points are connected using B-spline curves. A common problem when tracing centrelines is the possibility of loops being formed due to interactions with other vessels or irregularities in the image data. An alternative approach was presented by Wilson and Noble [34]. To extract the vascular network from the image data, an adaptive expectation maximization (EM) algorithm was presented that recursively divides the volume into smaller sub-volumes on which a localised segmentation was performed. The identified parameters for the distributions within a sub-volume, give indications of which tissues are present, and as such 'special' cases were applied for the classification of voxels. Variation in signal intensity is only expected for arteries, but not for the cerebrospinal fluid and brain tissue. In this the data differs

from soil-root samples, where the soil environment is found to be highly heterogeneous. Other complex root-structure-like networks are found, for instance, in neuronal arborescences [17].

3 Method

In this section we give a detailed description of the proposed extraction technique, beginning with the extraction of a single individual root system, assuming that all root cross-sections belong to the same plant. We introduce each of the components and how they are integrated into the tracking framework. A collision detection mechanism is then added to identify the interaction of multiple targets, to which a shape constraint is imposed, allowing the extraction of multiple interacting plant root systems. The objectives of the work reported here are to:

- identify the boundaries of root cross-sections
- track individual root cross-sections
- keep root cross-sections arising from different plants separate

3.1 Object Boundary Detection

We adopt the level set framework [28] to search for the boundaries of root cross-sections. We aim at finding the interface

$$C\left(t\right) = \left\{ \left(x, y\right) \middle| \Phi_{x,y,t} = 0 \right\} \tag{1}$$

of a time-dependent function $\Phi_{x,y,t}$ that separates an object consisting of comparable intensity values from its heterogeneous background. The interface of $\Phi_{x,y,t}$ can be implicitly propagated solving a partial differential equation

$$\frac{\partial \Phi_{x,y,t}}{\partial t} + F\left|\nabla \Phi_{x,y,t}\right| = 0 \tag{2}$$

which can be approximated and rewritten using a finite forward difference scheme in time

$$\frac{\Phi_{x,y}^{t+1} - \Phi_{x,y}^{t}}{\Delta t} + F\left|\nabla_{x,y} \Phi_{x,y}^{t}\right| = 0 \tag{3}$$

giving a general formulation of the time-discretized level set method, with F being a speed function that defines the motion of the front over time t. One possible way to find the boundary of an arbitrary object is to define a speed function that stops at high image gradients. A solution based on the formulation presented in [16] was tested, but failed to correctly identify root objects: blurred and low contrast boundaries are common in CT data. A solution is therefore proposed that evolves a level set function guided by a greyscale intensity distribution model. Assuming we have the greyscale intensity values of a known

root object, we use a kernel density estimator to build a statistical probability density function, which we will refer to as our root appearance model p_m

$$p_m(x) = \frac{1}{nh} \sum_{i=0}^{n} K\left(\frac{x - x\,(i)}{h}\right) \tag{4}$$

where n is the number of data points, h the bandwidth and K a Gaussian smoothing kernel $K(x) = \frac{1}{\sqrt{2\pi}} e^{-\frac{1}{2}x^2}$. Using the Jensen-Shannon (JS) divergence [13] as given in Equation 5, we compute the distance between a probability density function p_f estimated around the interface of the level set function and our known root model p_m.

$$JS(p_f, p_m) = H(w_1 p_f + w_2 p_m) - w_1 H(p_f) - w_2 H(p_m) \tag{5}$$

where H is the Shannon entropy function and calculated as in Equation 6. w_1 and w_2 are two weighting parameters $w_1, w_2 \geq 0, w_1 + w_2 = 1$ to balance the contribution of the two statistical probability density functions and useful for conditional probability studies where the weighting parameters represent prior probabilities. In our case, however, we set $w_1 = w_2 = 0.5$.

$$H(p) = -\sum_{i=0}^{n} p_i \; log_b\,(p_i) \tag{6}$$

The JS divergence is a non-negative and symmetric dissimilarity measure, bounded by $[0, log_b 2]$. Using a logarithm of base 2 results in a distance that is measured within $[0, 1]$, where 0 is considered a complete match between two probability density functions. The higher the value of the JS divergence the lower is the probability that the data come from the same distribution. These and the fact that the dissimilarity measure is not constrained by the number of samples and their shape of the distribution, makes the JS divergence a good choice in our application. Given the above definitions, we can now build them into a level set framework

$$\Phi_{x,y}^{t+1} = \Phi_{x,y}^{t} + \Delta t \left[-(\alpha)\left(JS_{\beta\vee}\nabla^{+} + JS_{\beta\wedge}\nabla^{-}\right) + (1-\alpha)\,(\kappa)\right] \tag{7}$$

where $JS_{\beta\vee} = max\,(\lceil \beta - JS \rceil, 0)$ and $JS_{\beta\wedge} = min\,(\lfloor \beta - JS \rfloor, 0)$ are the propagation forces, with $\beta \in [0, 1]$ defining the acceptance distance of the JS divergence between model and data distribution. $\alpha \in [0, 1]$ is a weighting parameter between the propagation force and the curvature dependency $\kappa = \nabla \cdot \frac{\nabla \Phi_{x,y}^{t}}{\left|\nabla \Phi_{x,y}^{t}\right|}$ of the front. The numerical solution requires choosing the correct difference scheme that propagates information in the direction upwind to the moving interface. This is achieved through $\nabla^{+} = \sqrt{max(D^{-x,y}, 0)^2 + min(D^{+x,y}, 0)^2}$ in case of an expanding force and similarly through $\nabla^{-} = \sqrt{max(D^{+x,y}, 0)^2 + min(D^{-x,y}, 0)^2}$ for a contracting force, where $D^{+x} = \frac{\Phi_{x+\Delta x,y,t} - \Phi_{x,y,t}}{\Delta x}$ is the forward difference operator and $D^{-x} = \frac{\Phi_{x,y,t} - \Phi_{x-\Delta x,y,t}}{\Delta x}$ the backward difference operator. The level set framework is implemented using the narrow band strategy [4] for increased

efficiency and the fast sweeping method [36] for re-initialisation. Figure 1 shows a cross-sectional image in which root objects are identified and separated from their complex and heterogeneous soil environment using the above described method.

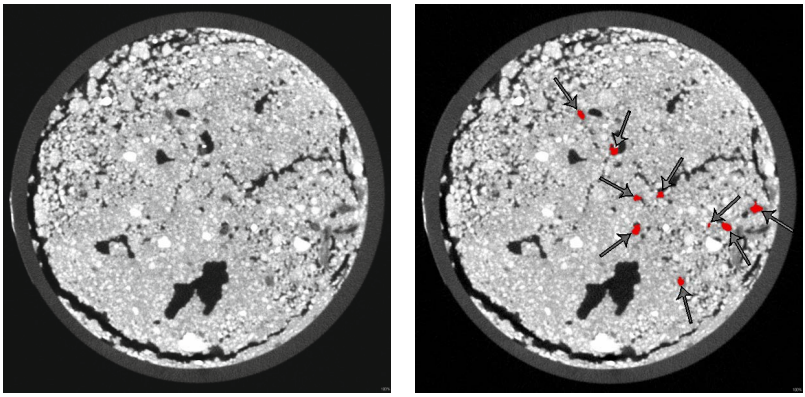

(a) **(b)**

Fig. 1. Cross-sectional image of (a) raw data and (b) with identified root objects

3.2 Tracking Root Objects

Target objects are selected for tracking by the user manually setting seed points in the first (top) image in the stack. An initial root appearance model is built for each target from the greyscale intensity values within a 5 pixel radius. The seed points also mark the initial interface of the propagating level set function, which is evolved until the root object boundaries are identified. Since a level set function can implicitly represent multiple interfaces, a classical two-pass connected component algorithm [23] is used to assign a label to each object. Labels are propagated when constructing the narrow band around an interface and it is therefore possible to evolve the level set function using different appearance models for each root object. This means that we do not have a single model that represents all the root objects in a plant at the same time, but several models that are generated, each representing a single target (root segment).

Once the boundaries of root objects are identified, the aim is to track target objects through a sequence of horizontal slices, or images, thereby building up a three-dimensional segmentation of the root system. Due to the high resolution of X-ray μCT data, we assume that corresponding root locations in consecutive images partially overlap, and that their greyscale intensity distributions vary smoothly. Some variation is to be expected due to the heterogeneous environment of different density materials and unevenly distributed water content in the soil throughout the sample and the root system, which can vary the overall estimated attenuation of the voxel data. Therefore, as root objects are followed through

the image sequence, their assigned root model distribution must be updated to adapt to their changing appearance. This is done by re-computing the root appearance model from the greyscale intensity values enclosed by each of the converged interfaces of the level set function.

Updating the root model is an inevitable step, yet it conceals potential problems. Noise or small areas of background might be included within the interface and so contribute to its probability density function. These errors can accumulate and result in a model that is no longer an appropriate representation of a tracked root object. Therefore, to reduce the potential of model drift, we use a complex Fourier shape descriptor [8] to compare the shape of a root object in pairs of consecutive images and only update the root appearance model when the sum of squared differences of their filtered and normalised power spectra is below a given threshold.

A root system is composed of several branching roots. Splitting of a root boundary as it branches throughout the image stack is implicitly dealt with by the level set's ability to adapt to changing topologies. As the level set interface evolves from one state to another it can split into multiple disjoint interfaces. When a target object separates, the level set evolves based on the same root model, but will become two independent objects with their own updating root appearance model after proceeding to the next image slice. Figure 2 shows a sequence of cross-sectional images in which root objects are followed.

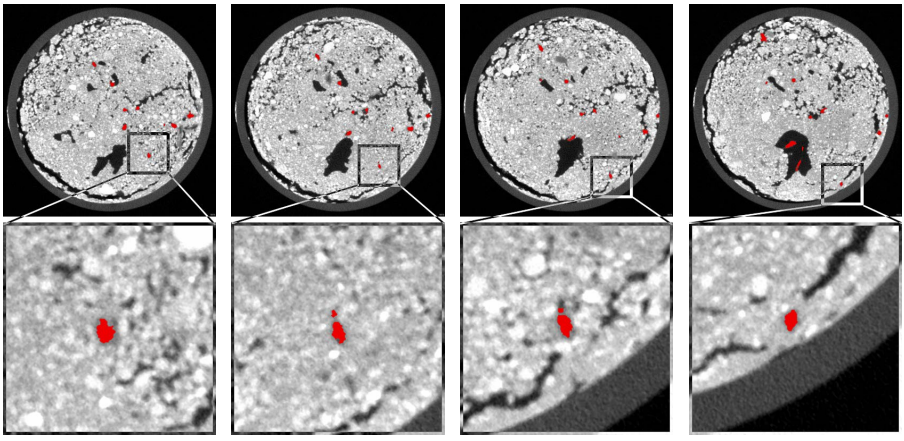

Fig. 2. Sequence of cross-sectional images with target objects highlighted and followed shown at an interval of every 40 image slices

3.3 Multiple Interacting Objects

To extract multiple root systems, a level set tracker is initialised to each plant and their level set functions evolved simultaneously. In this work we adopt the concept of multiple level set functions as presented in [27]. Let Φ_A^t and Φ_B^t be

two level set functions and their interfaces occupy two different regions at time step t. The level set functions evolve separately, based on their individual root appearance models, resulting in a temporary state of Φ_A^* and Φ_B^*. Φ_A^* and Φ_B^* are then combined to obtain the level set functions Φ_A^{t+1} and Φ_B^{t+1} at time $t+1$. The combination of the temporary level set functions depends on whether or not the interface of A can penetrate the interface of B, or vice versa, and as such pushes back the adjacent interface. Assuming that A can penetrate B, but B cannot penetrate A, then the new level set function at time step $t+1$ will be updated accordingly:

$$\begin{aligned} \Phi_A^{t+1} &= \Phi_A^* \\ \Phi_B^{t+1} &= \max\left(\Phi_B^*, -\Phi_A^*\right) \end{aligned} \tag{8}$$

This example should make it easy to understand how interacting level set fronts can be controlled and how this can be modified to define similar rules such that during an encounter of two level set fronts, neither is allowed to penetrate the other. This will stop them from advancing further and give an exact partition of the two regions at the front of collision. The mechanism of multiple fronts can be easily extended to any number of level set functions using the same principles of combination. Each evolving front in the set must be compared to all other level set functions of the same set. This easily allows identification of any collisions between interfaces and determination of which of the level set functions interact. Figure 3 shows three different scenarios where two level set functions (front A (red) and front B (blue)) are evolved until their fronts interact with each other, at which point different combination rules are applied. This is a key element in the extraction of multiple interacting root systems, but not sufficient to allow separation of interacting root systems. While the combination rules allow individual trackers to be separated, the true boundary between touching root cross-sections remains unknown. Although level set functions can penetrate each other's interface, there is no definition given yet of when these rules are to be applied. For this, shape information is used to estimate the boundary of root objects and so to find the intersecting front between them.

While tracking target objects through the image stack, their shape is noted and used to control appearance model updates. We can, therefore, easily recall an object's outline and store the most recent shape information before the interaction with other objects. This information is kept until the interaction ceases. Let $U = \{\boldsymbol{u}_i | i = 1..N_u\}$ be a set of data points along the outline of a stored shape and $V = \{\boldsymbol{v}_i | i = 1..N_v\}$ be a set of data points along a level set's interface. The rotation matrix $\mathbf{R}$ and the translation matrix $\mathbf{T}$ are sought to minimise the root mean squared distance between U and V and therefore to find the best alignment of the two point sets. This can be achieved using the iterative closest point (ICP) algorithm [2]. By calculating the centre of mass $\boldsymbol{\mu_u}$ and $\boldsymbol{\mu_v}$ of the two point clouds, it is possible to determine the cross-covariance matrix $cov_{uv} = \frac{1}{N_u} \sum_{i=1}^{N_u} [(\boldsymbol{u}_i - \boldsymbol{\mu_u})(\boldsymbol{v}_i - \boldsymbol{\mu_v})^\intercal]$ for U and V. Using the cyclic components $\boldsymbol{a} = (A_{23}, A_{31}, A_{12})$ of a matrix $\mathbf{A} = cov_{uv} - cov_{uv}^\intercal$ allows the definition of a 4×4 matrix $\mathbf{Q}$

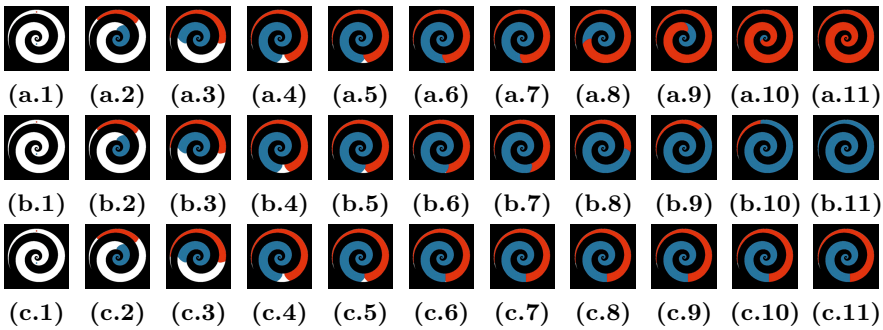

Fig. 3. Two level set function A (red) and B (blue) interacting with each other, where (a) front A penetrates front B, (b) front B penetrates front A and (c) neither A or B is penetrated

$$\mathbf{Q}_{4\times4} = \begin{pmatrix} tr(cov_{uv}) & \boldsymbol{a}^{\intercal} \\ \boldsymbol{a} & cov_{uv} + cov_{uv}^{\intercal} - tr(cov_{uv})\mathbf{I}_3 \end{pmatrix} \tag{9}$$

The eigenvector $\boldsymbol{r} = (q_1 \quad q_2 \quad q_3 \quad q_4)$ of the matrix $\mathbf{Q}$ with the maximum eigenvalue is used to define the rotation matrix $\mathbf{R}$

$$\mathbf{R} = \begin{pmatrix} q_1^2 + q_2^2 - q_3^2 - q_4^2 & 2(q_2q_3 - q_1q_4) & 2(q_2q_4 + q_1q_3) & 0 \\ 2(q_2q_3 + q_1q_4) & q_1^2 + q_3^2 - q_2^2 - q_4^2 & 2(q_3q_4 - q_1q_2) & 0 \\ 2(q_2q_4 - q_1q_3) & 2(q_3q_4 + q_1q_2) & q_1^2 + q_4^2 - q_2^2 - q_3^2 & 0 \\ 0 & 0 & 0 & 1 \end{pmatrix} \tag{10}$$

The vector $\boldsymbol{t} = (\boldsymbol{\mu_v} - \mathbf{R}\boldsymbol{\mu_u})$ is used to define the translation matrix $\mathbf{T}$

$$\mathbf{T} = \begin{pmatrix} 1 & 0 & 0 & t_1 \\ 0 & 1 & 0 & t_2 \\ 0 & 0 & 1 & t_3 \\ 0 & 0 & 0 & 1 \end{pmatrix} \tag{11}$$

The ICP algorithm is initialised by setting the rotation and translation matrices equal to the identity matrix $\mathbf{R} = \mathbf{T} = \mathbf{I}$ and begins by identifying for each point $\boldsymbol{u} \in U$ the best match with the shortest distance $d(\boldsymbol{u}, V) = min_{\boldsymbol{v}\in V}\|\boldsymbol{v}-\boldsymbol{u}\|$. This step can be efficiently performed using a k-d tree [25]. With the set of matching pairs as input, the best registration is calculated using the quaternion-based least square method, determining $\mathbf{R}$ and $\mathbf{T}$ which are then applied to U. The whole process is repeated iteratively, finding new matching points and their transformation, until the change in mean squared error falls below a given threshold.

When the interfaces of two level set functions collide, and each is made impenetrable, race conditions are generated, as illustrated in Figure 4. This, however, can be solved using shape constraints. The ICP algorithm, as described above, is used to find the best alignment of the stored shape to the evolving interface. This leaves each point within the interface in one of two possible states: it is

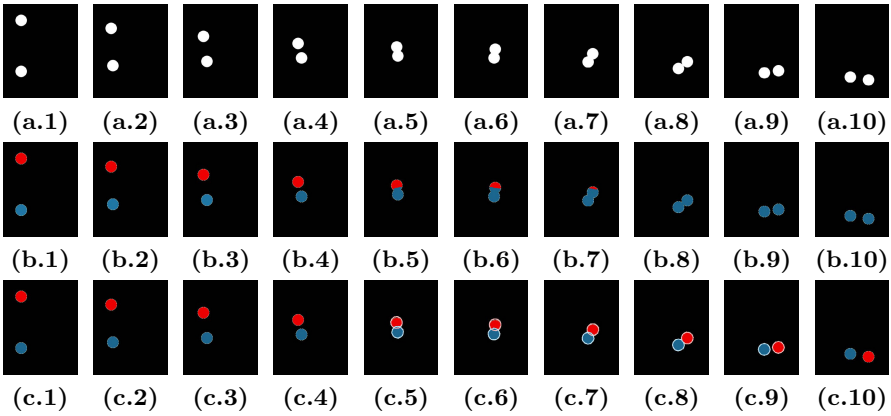

Fig. 4. Two colliding target objects; (a) raw data, (b) extracted using the conventional level set tracking approach and (c) combined with the ICP algorithm during the period of contact (5-9)

either outside or inside of its aligned region. Let $S = \{S_1..S_n\}$ be the enclosed areas of each aligned shape to its corresponding level set function, $L = \{\Phi_1..\Phi_n\}$ be the set of level set functions at time t and $L^* = \{\Phi_1^*..\Phi_n^*\}$ the set of their temporary states, then the final value of the level set function Φ_i^{t+1} at time step $t+1$ and position p is updated accordingly

$$\Phi_i^{t+1} = \begin{cases} \Phi_i^* & \text{if } (p \in S_i) \wedge (p \notin \{S \backslash S_i\}) \\ \max\left(\Phi_i^*, -\{L_j | p \in S_j\}\right) & \text{if } (p \in S_i) \wedge (p \cap \{S \backslash S_i\} \neq \emptyset) \\ \max\left(\Phi_i^*, -\{L^* \backslash \Phi_i^*\}\right) & \text{if } (p \cap S_i = \emptyset) \end{cases} \tag{12}$$

A particular benefit of this solution is that, while it constrains the movement of the front, the selected root object is not required to maintain the registered shape. This allows the detection of lateral roots, since a level set function can still evolve beyond the aligned region. At the same time it prevents the path of a level set function being blocked by faster evolving level sets and allows their interface to be penetrated so that control over its target is maintained. The effect of adding shape constraints to the level set functions is illustrated in Figure 4. Figure 5 shows a sequence of images in which tracked root cross-sections interact with each other.

4 Experiment

Winter wheat Cordiale (*Triticumaestivum L.*) were grown in columns of 30mm and 60mm in diameter filled with soil. Two each of the four 30mm columns were filled with loamy sand and clay loam. The 60mm column was filled with loamy sand. The soil was air-dried and sieved to <2mm. The seeds were germinated in Petri dishes on wet filter papers, covered with an aluminium foil to shield them

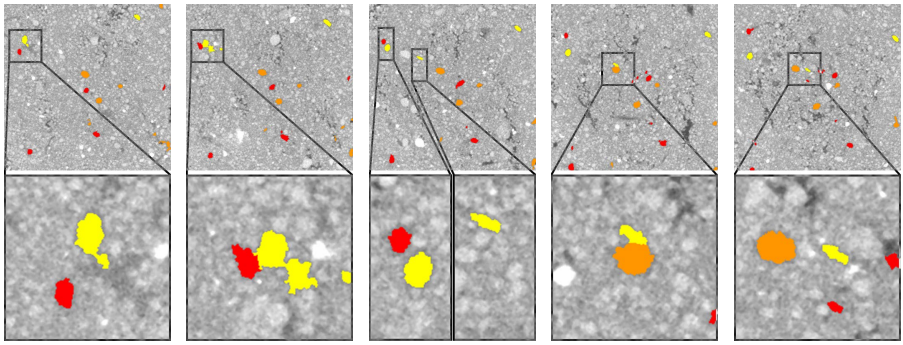

Fig. 5. Sequence of cross-sectional images with multiple and interacting target objects highlighted and followed shown at an interval of every 20-40 image slices

from sunlight, and planted after two days. A single seed was placed in each of the 30mm columns, while three seeds were placed 10mm to 15mm apart from each other in the 60mm column. The plants grew in environmental controlled growth rooms with 16/8 hours light cycle at a temperature of 23/18 degree Celsius and were scanned ten days after germination. The water status of the samples at the point of imaging was approximately at field capacity.

The imaging device used in this experiment was a Nanotom (Phoenix X-ray/GE Measurement & Control Systems) X-ray μCT scanner. The scan for the 30mm columns was performed at 120keV and 250μA, taking 1,200 projections at an exposure time of 750ms, using a signal averaging of 3 and 1 skipping per projection. A 0.1mm Cu filter was used to harden the beam. Samples were placed 200mm away from the X-ray gun, resulting in a volume with resolution of 25.0μm voxel size and an image stack of 1,400×1,400×2,200 voxels. The scan for the 60mm column was performed at 130keV and 200μA, taking 1440 projections at an exposure time of 1,000ms, using a signal averaging of 4 and 1 skipping per projection. A 0.2mm Cu filter was used to harden the beam. The sample was placed 220mm away from the X-ray gun, resulting in a volume with resolution of 27.5μm voxel size and an image stack of 2,100×2,100×2,260 voxels. The acquired volume data was saved to a stack of 8-bit images. The tracking framework proposed here was used to recover the root systems from the image data. Seed points were selected manually in the first image of each stack to mark target objects and to initialise separate trackers to each of the root systems.

Figure 6 shows the rendered images of the extracted root systems of the individually grown wheat plants. After scanning the samples with X-ray μCT, they were root-washed free of soil, placed on a water tray and imaged with a flatbed scanner at 400dpi. The two-dimensional images are shown as reference to the extracted data. The figures in comparison show that the overall architecture of the root systems has been captured successfully. It has been proven to be difficult to recover all of the fine lateral roots of the root system at this resolution

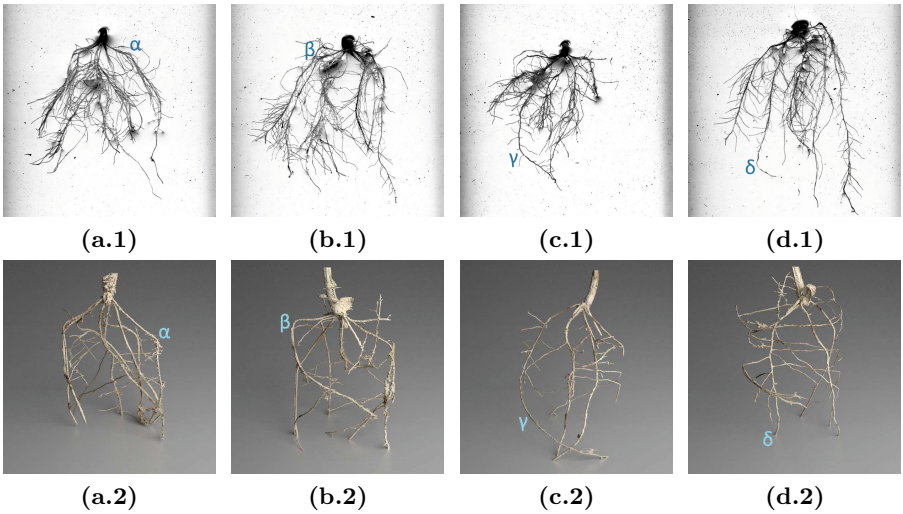

Fig. 6. Extracted root systems of wheat grown in (a-b) loamy sand and (c-d) clay loam, (x.1) imaged for comparison with a flatbed scanner and (x.2) the rendered root systems extracted from X-ray μCT data using α, β, γ and δ for alignment reference. The root systems in (x.1) once extracted from the soil, lost their three-dimensional geometry information, while still preserved in (x.2)

of scanning. While some might not be visible in the image data, due to their small size, others might be present, but not necessarily shown as connected due to disruptions caused by small image irregularities. The extracted root systems from the sample of multiple interacting plants are shown in Figure 7, highlighting each of the three root systems separately in a different colour.

Fig. 7. Extracted root systems of multiple interacting wheat plants (a) all together, (b) highlighted first, (c) second and (d) third root system

5 Discussion and Conclusions

We have presented a visual object tracking framework for the extraction of plant root systems grown in soil from X-ray μCT volume data, allowing the recovery of both individual and multiple interacting plant root systems. The method proposed here uses a modified level set framework that is guided by a greyscale intensity distribution model to find the boundaries of root cross-sections. The appearance model is updated to adapt to variations in the greyscale intensity values of the target object. The interface of a level set function is continuously readjusted to locate the new position and outline of the target objects in subsequent images. After following root cross-sections through the image stack, the extracted information is used to reassemble the complete root system of a plant.

In the presence of multiple root systems, multiple trackers are deployed, but need to be able to keep their targets distinguished from each other. This is challenging since root cross-sections are likely to share similar, if not identical, greyscale intensity distributions and hence the appearance model used by the trackers is not enough to keep the objects separate. Shape constraints are therefore added when objects interact, and help lock the trackers to their correct targets.

The method proposed here was tested on root systems of winter wheat Cordiale (*Triticumaestivum L.*), using data showing individual as well as multiple interacting root systems. Results show that the proposed technique can successfully recover and separate plant roots from each other and therefore increase the likelihood of the assigned roots belonging to the originating plant.

As more mature plant root systems are examined, larger columns are needed to provide enough space for the root system to explore the soil environment. When using larger samples, scan resolution will be compromised, resulting in more disjoint root segments. While at present an adaptive appearance model is used by the tracking framework, its motion model is still very simplistic, relying on the assumption that root cross-section will partially overlap in consecutive images. This assumption might not hold if larger samples are used. Hence a more sophisticated motion model will be required. Another compromise in using larger sample sizes is that more fine lateral roots will become unidentifiable due to the reduction in resolution. These issues will be the subject of future reports.

Acknowledgments. This work was supported by Biotechnology and Biological Sciences Research Council and Engineering and Physical Sciences Research Council Centre for Integrative Systems Biology program funding to the Centre for Plant Integrative Biology; European Research Council Advanced Grant funding to M.J.B., T.P.P., S.J.M., C.J.S., S.M.; BBSRC Professorial Fellowship funding to M.J.B.; Belgian Science Policy Office (grant IAP7/29) funding to M.J.B.; Royal Society Wolfson Research Merit Award to M.J.B.; EU FP7-KBBE-2011-5 project EURoot: Enhancing resource uptake from roots under stress in cereal crops to T.P.P. and M.J.B.

References

1. Aykac, D., Hoffman, E., McLennan, G., Reinhardt, J.: Segmentation and analysis of the human airway tree from three-dimensional X-ray CT images. IEEE Transactions on Medical Imaging **22**(8), 940–950 (2003)
2. Besl, P.J., McKay, N.D.: A method for registration of 3-D shapes. IEEE Transactions on Pattern Analysis and Machine Intelligence **14**(2), 239–256 (1992)
3. Chéné, Y., Rousseau, D., Lucidarme, P., Bertheloot, J., Caffier, V., Morel, P., Belin, Í., Chapeau-Blondeau, F.: On the use of depth camera for 3D phenotyping of entire plants. Computers and Electronics in Agriculture **82**, 122–127 (2012)
4. Chopp, D.L.: Computing minimal surfaces via level set curvature flow. Journal of Computational Physics **106**(1), 77–91 (1993)
5. Clark, R.T., MacCurdy, R.B., Jung, J.K., Shaff, J.E., McCouch, S.R., Aneshansley, D.J., Kochian, L.V.: Three-dimensional root phenotyping with a novel imaging and software platform. Plant Physiology **156**(2), 455–465 (2011)
6. Crowell, S., Falcao, A.X., Shah, A., Wilson, Z., Greenberg, A.J., McCouch, S.R.: High-resolution inflorescence phenotyping using a novel image analysis pipeline, panorama. Plant Physiology (2014)
7. Flasque, N., Desvignes, M., Constans, J.M., Revenu, M.: Acquisition, segmentation and tracking of the cerebral vascular tree on 3D magnetic resonance angiography images. Medical Image Analysis **5**(3), 173–183 (2001)
8. Granlund, G.H.: Fourier preprocessing for hand print character recognition. IEEE Transactions on Computers **C–21**(2), 195–201 (1972)
9. Heeraman, D.A., Hopmans, J.W., Clausnitzer, V.: Three dimensional imaging of plant roots in situ with X-ray computed tomography. Plant and Soil **189**, 167–179 (1997)
10. Hinsinger, P., Gobran, G.R., Gregory, P.J., Wenzel, W.W.: Rhizosphere geometry and heterogeneity arising from root-mediated physical and chemical processes. New Phytologist **168**(2), 293–303 (2005)
11. Kaestner, A., Schneebeli, M., Graf, F.: Visualizing three-dimensional root networks using computed tomography. Geoderma **136**(12), 459–469 (2006)
12. Khan, Z., Balch, T., Dellaert, F.: MCMC-based particle filtering for tracking a variable number of interacting targets. IEEE Transactions on Pattern Analysis and Machine Intelligence **27**(11), 1805–1819 (2005)
13. Lin, J.: Divergence measures based on the shannon entropy. IEEE Transactions on Information Theory **37**(1), 145–151 (1991)
14. Lontoc-Roy, M., Dutilleul, P., Prasher, S.O., Han, L., Brouillet, T., Smith, D.L.: Advances in the acquisition and analysis of CT scan data to isolate a crop root system from the soil medium and quantify root system complexity in 3-D space. Geoderma **137**(12), 231–241 (2006)
15. Lynch, J.P.: Root architecture and plant productivity. Plant Physiology **109**(1), 7–13 (1995)
16. Malladi, R., Sethian, J.A., Vemuri, B.C.: Shape modeling with front propagation: a level set approach. IEEE Transactions on Pattern Analysis and Machine Intelligence **17**(2), 158–175 (1995)
17. Meijering, E.: Neuron tracing in perspective. Cytometry Part A **77A**(7), 693–704 (2010)
18. Meyer, F.: Contrast features extraction. SPIE Milestone Series **127**, 139–145 (1996)
19. Mooney, S.J., Pridmore, T.P., Helliwell, J., Bennett, M.J.: Developing X-ray computed tomography to non-invasively image 3-D root systems architecture in soil. Plant and Soil **352**, 1–22 (2012)

20. Perret, J.S., Al-Belushi, M.E., Deadman, M.: Non-destructive visualization and quantification of roots using computed tomography. Soil Biology and Biochemistry **39**(2), 391–399 (2007)
21. Pierret, A., Capowiez, Y., Moran, C.J., Kretzschmar, A.: X-ray computed tomography to quantify tree rooting spatial distributions. Geoderma **90**(34), 307–326 (1999)
22. Price, C.A., Symonova, O., Mileyko, Y., Hilley, T., Weitz, J.S.: Leaf extraction and analysis framework graphical user interface: Segmenting and analyzing the structure of leaf veins and areoles. Plant Physiology **155**(1), 236–245 (2011)
23. Rosenfeld, A.: Connectivity in digital pictures. Journal of the ACM **17**(1), 146–160 (1970)
24. Rosin, P.L.: Unimodal thresholding. Pattern Recognition **34**(11), 2083–2096 (2001)
25. Rusinkiewicz, S., Levoy, M.: Efficient variants of the ICP algorithm. In: 2001 Proceedings of the Third International Conference on3-D Digital Imaging and Modeling, pp. 145–152 (2001)
26. Schenk, H.J.: Root competition: beyond resource depletion. Journal of Ecology **94**(4), 725–739 (2006)
27. Sethian, J.A.: Level set techniques for tracking interfaces: Fast algorithms, multiple regions, grid generation and shape/character recognition. In: Proceedings of the International Conference on Curvature Flows and Related Topics, Trento, Italy, pp. 215–231 (1994)
28. Sethian, J.A.: Level Set Methods and Fast Marching Methods: Evolving Interfaces in Computational Geometry, Fluid Mechanics, Computer Vision, and Materials Science.. on Applied and Computational Mathematics, 2nd edn. Cambridge University Press (1999)
29. Sonka, M., Hlavac, V., Boyle, R.: Image Processing, Analysis, and Machine Vision. Chapman and Hall (1993)
30. Sonka, M., Park, W., Hoffman, E.A.: Rule-based detection of intrathoracic airway trees. IEEE Transactions on Medical Imaging **15**(3), 314–326 (1996)
31. Trachsel, S., Kaeppler, S., Brown, K., Lynch, J.: Shovelomics: high throughput phenotyping of maize (Zea mays L.) root architecture in the field. Plant and Soil **341**(1–2), 75–87 (2011)
32. Tschirren, J., Hoffman, E., McLennan, G., Sonka, M.: Intrathoracic airway trees: segmentation and airway morphology analysis from low-dose CT scans. IEEE Transactions on Medical Imaging **24**(12), 1529–1539 (2005)
33. Vincent, L.: Morphological grayscale reconstruction in image analysis: applications and efficient algorithms. IEEE Transactions on Image Processing **2**(2), 176–201 (1993)
34. Wilson, D.L., Noble, J.A.: An adaptive segmentation algorithm for time-of-flight MRA data. IEEE Transactions on Medical Imaging **18**(10), 938–945 (1999)
35. Zappala, S., Helliwell, J.R., Tracy, S.R., Mairhofer, S., Sturrock, C.J., Pridmore, T., Bennett, M., Mooney, S.J.: Effects of X-ray dose on rhizosphere studies using X-ray computed tomography. PloS one **8**(6), e67250 (2013)
36. Zhao, H.: A fast sweeping method for eikonal equations. Mathematics of computation **74**(250), 603–628 (2005)